Automated method for routine microplastic detection and quantification

Automated method for routine microplastic detection and quantification

Matteo Giardino[1,2], Valentina Balestra[3],*, Davide Janner[1,2], Rossana Bellopede[3]

[1]Department of Applied Science and Technology (DISAT), Politecnico di Torino, Corso Duca degli Abruzzi 24, 10129 Torino, Italy, matteo.giardino@polito.it [0000-0003-1492-2498], davide.janner@polito.it [0000-0001-7954-979X]

[2]INSTM, Consorzio Interuniversitario Nazionale per la Scienza e Tecnologia dei Materiali, Via G. Giusti 9, 50121 Florence, Italy, matteo.giardino@polito.it, davide.janner@polito.it

[3]Department of Environment, Land and Infrastructure Engineering (DIATI), Politecnico di Torino, Corso Duca degli Abruzzi 24, 10129 Torino, Italy, valentina.balestra@polito.it [0000-0002-8529-468X], rossana.bellopede@polito.it [0000-0002-9569-0678]

* Corresponding author

Abstract

Microplastics (MPs) are a heterogeneous group of solid polymers with dimensions less than 5 mm, which are a widespread contaminant of the environment. Their ubiquitous presence grabbed researchers' attention in the last decade, and the problem of MPs detection and quantification is currently a topic of utmost importance. Most identification and quantification protocols are still based on the visual count, which is an extremely time-consuming and error-prone task due to operator subjectivity. To address such an issue, different software analysis procedures are available, but they mainly rely either on the use of optical microscopy, covering a minimal area for each sample (mm² size), or they allow only the identification of the largest particles (>1mm). Here, a semi-automatic innovative image processing method for quantifying and measuring microplastics on filter membrane substrates is presented and validated, comparing results with data obtained using visual counting performed by an experienced operator. The algorithm was tested with artificially generated microplastic images and samples taken from natural environments. Samples of Borgio Verezzi show cave sediment and Po River water were filtered on a glass filter membrane, and

photographs were taken under 365 nm illumination, both without and with Nile Red staining. The proposed image analysis method, implemented in an easy-to-use Python script, was quite accurate and fast (about 10 s/image average processing time), showing an average deviation below 10%, which is further reduced to about 8% if the samples are stained with Nile Red.

KEYWORDS: Microplastic pollution, staining dye, fluorescence, water and sediment monitoring, image analysis

1. Introduction

Microplastics (MPs) are a heterogeneous group of solid polymers generally considered with a dimension less than 5 mm by the scientific community, originating from primary production or from the fragmentation of larger plastics (secondary production) (Corami et al., 2020). MPs lead to environmental contamination worldwide (Ha and Yeo, 2018) and have been widely found in marine and terrestrial environments, even transported in the air (Balestra and Bellopede, 2022; Boyle and Örmeci, 2020; Chia et al., 2021; Cutroneo et al., 2020; Guerranti et al., 2017; Huang et al., 2021; Ren et al., 2021; Samandra et al., 2022; Zhang et al., 2019).

Monitoring MP pollution in the environment is essential to understand better their sources and their impacts on ecosystems and human health (Barboza et al., 2018; Henry et al., 2018; Prata et al., 2019; Sharma and Chatterjee, 2017). Despite a large consensus in recognizing the importance of MPs monitoring protocols, there is no universal methodology for analyzing MPs. The visual identification method for counting and sorting MPs based on color, size, and shape, is one of the most commonly used (Alomar et al., 2016; Balestra and Bellopede, 2022; Cannas et al., 2017; Hidalgo-Ruz et al., 2012; Mathalon and Hill, 2014), given its inexpensive and relatively rapid implementation (Crawford and Quinn, 2016). However, such a technique is highly susceptible to operator biases and errors, thus frequently leading to misidentification (Crawford and Quinn, 2016; Prata et al., 2019). In fact, it was demonstrated that the visual

count by two different expert operators could differ even up to 30% from each other (Esch et al., 2020). As an improvement to the process, staining dyes, such as Nile Red, are commonly used to increase the visual identification efficacy of MPs by conferring color or fluorescence to the particles (Erni-Cassola et al., 2017; Prata et al., 2019).

A similar effect can be obtained by exploiting the fluorescence given by fluorescent whitening agents (FWAs) that are often used in plastic production (Qiu et al., 2015). Indeed, MPs with FWAs or after fluorescent dye application can easily be detected under a fluorescence microscope or a low-cost ultraviolet (UV) flashlight (Balestra and Bellopede, 2022; Ehlers et al., 2020; Klein and Fischer, 2019).

Based on their color or fluorescence, MPs could be photographed and automatically quantified by software identification, possibly removing the operator biases, and reducing the processing time, thus enabling faster processing than traditional methods. For those reasons, recently, there has been an increasing interest in image analysis techniques for MPs characterization (Gauci et al., 2019; Lorenzo-Navarro et al., 2021, 2020; Mukhanov et al., 2019; Prata et al., 2020, 2019; Wegmayr et al., 2020). The Image-J software was used by Mukhanov et al. (2019) to classify MPs into different classes, and the Microplastics Visual Analysis Tool (MP-VAT) was created by Prata et al. (2019) to automatically count fluorescent MPs stained with Nile Red dye under a specific wavelength illumination. However, different factors, such as the staining process, camera conditions and settings, introduce variability in the outcomes, thus requiring improvements that were subsequently implemented in another release of the software (MP-VAT 2.0) (Prata et al., 2020).

Using a MATLAB-based software (Gauci et al., 2019), MP particles extracted from samples originating from different beaches were characterized. Lorenzo-Navarro et al. (2020) counted and classified MPs particles using as input two images acquired with a high-resolution flat scanner and their System for Microplastics Automatic Counting and Classification (SMACC). Deep learning applications for MPs analysis have been employed to segment synthetic fibers in microscopy images (Wegmayr et al., 2020) and count and classify MPs using pictures taken with cameras or mobile phones (Lorenzo-Navarro et al., 2021). However, all these programs are often tested on samples created in the laboratory

or images taken from plastic fragments cut in controlled environments, not considering the difficulties of analyzing real samples. In images or samples created in a laboratory, MPs can be positioned very far from each other, there are no overlaps of particles, and the contours of the particles are well-defined (e.g. Lorenzo-Navarro et al, 2020). Moreover, sometimes only particles with larger dimensions are counted (e.g. Lorenzo-Navarro et al, 2020; Gauci et al., 2019). On the contrary, in real samples, particles overlap is frequently observed, and MPs are subject to erosion and biofouling, which often change their shape, color, and contours.

Moreover, the number of microplastics in real samples is often higher than those considered in the created images or samples. Finally, laboratory samples have no disturbing factors, while real samples often have particles and sediment powders that can make the background less uniform and clear for the optimal visualization of the particles. One of the last developments consist of a thresholding approach for fluorescence microscope images proposed by Meyer et al. (2022), where machine learning techniques are also employed for the classification of the different typologies of plastics.

Unfortunately, machine learning classification requires supervised training on large datasets, and most of these techniques may not perform well on real-world images if they are too different from training ones, especially when trying to detect and classify tiny and small-resolution objects in a vast uncorrelated background (Liu et al., 2021).

The present work aims to develop an automated counting software using images taken with cameras on filters of real samples selected in different matrices, limiting subjectivity in quantifying MPs particles and reducing the processing time compared to traditional methods. The adopted approach relies on traditional image processing techniques where the user tunes process parameters without the need to train the software on microplastic sample images.

The software is provided with a very easy-to-use graphical user interface (GUI) which drives the operator along all the process workflow and makes it suitable for use by inexpert researchers. The automated counting has been applied to images created with both artificial (created by an image editing software) and real samples of Borgio Verezzi show cave sediments and Po River water collected inside the city of Turin.

2. Materials and methods

2.1. Sampling, laboratory analysis and methods

For all steps, plastic equipment was avoided or replaced with non-plastic utensils. All samples were collected in glass jars and stored at 6°C until laboratory analysis. The samples were selected in two different media (water and sediment), in two different environments (open river, underground cave) to demonstrate that the algorithm can be used effectively in all types of samples, regardless of matrix or environment. The samples collected from Borgio Verezzi show cave sediments and Po River waters were treated in the laboratory with the method described in Balestra and Bellopede, 2022, improved and adapted to the specific characteristics of the matrices. Borgio Verezzi dried cave sediments, particularly rich in organic matter, were subjected to organic matter removal through the application of 30% hydrogen peroxide solution, added in 1:1 sample volume ratio, and left to act at room temperature for 5 days. Po River samples were subjected to organic matter removal through the application of 30% hydrogen peroxide solution, added in 1:10 sample volume ratio, and left to act at room temperature for 5 days. The filters were photographed under the same conditions and then observed under a microscope to obtain the abundance and characterization of MPs. Finally, all filters were stained with Nile Red dye to evaluate a possible improvement of the images to be used in the software. A volume of 1 mL of Nile Red dye solution in Acetone (1:10µg/mL) was pipetted to cover all the filters and was left to dry for 30 minutes at room temperature, covered with aluminum foil. The filters were then dried further for 1 h at 40 ◦C in an oven.

The MPs on filters were observed with a UV flashlight (Alonefire SV10 365 nm UV flashlight 5W) under a LeitzORTHOLUX II POL-MK microscope equipped with a DeltaPix Invenio12EIII 12 Mpx Camera, with high magnifications, following the identification method described in Crawford & Quinn, 2016

2.2. Images setting and identification of microplastics

The quantification of microplastics may be influenced by the time between sample preparation and the identification of fluorescent particles (Prata et al., 2020). This can result in a relevant miscounting of MP

due to the loss of dye fluorescence, particles, or a combination of both over time. Therefore, visual identification and photographs were taken the day after filtration.

The intensity of fluorescence produced by MPs is dependent on the luminous emittance of the LED lantern used; thus, the UV LED light used to detect and photograph MPs was continuously connected to the power line electricity.

Camera conditions are important when using photographs in the identification of fluorescent MPs. Evaluation of digital photographs obtained with different cameras, also during the same day (morning, noon, afternoon) and following days, can lead to variations in the quantification of particles (Prata et al., 2020). Therefore, the same camera is used for the same tests; on the same day.

Different factors can cause errors during the creation of the photographs, such as temperature, influencing digital camera sensor (Theuwissen, 2008, 2007), presence of visible light, reducing the contrast between particle and background, focus and stabilization of the camera, which should be kept as constant as possible(Prata et al., 2020). Picture size could also lead to the loss of particles in lower resolutions, therefore, the acquired filter membrane area in the final photograph should be maximized to produce the most reliable results (Prata et al., 2020). No significant variations in temperature and contamination with visible light are expected in the controlled environment of the dark-room used for the assays. Filters were photographed with a high-definition SLR camera (Sony ILCE-7RM3 v 1.01) equipped with a Zeiss 100 mm macro1:2 fixed vertically with an Emlid pedestal under a UV flashlight (Alonefire SV10 365 nm UV flashlight 5W) placed on a laboratory stand with clamp, with an inclination of 45° at a fixed distance. Images were taken using an exposition of -2, 200 ISO, exposure time 0.62s, and diaphragm aperture f9 and f8 for filters with and without Nile Red, respectively. The camera was stabilized, photographs were taken under constant conditions and only working operators were allowed in the room to reduce potential light pollution.

Six images were created with image editing software (artificial samples), using the *clone* tool. In this way, MPs extracted from photos of real samples were copied and randomly positioned on an empty membrane

filter picture. These pictures, with a very uniform background and no disturbance from other fluorescent particles, are very useful to evaluate first the performance of the automated counting software.

MPs on six filters from Borgio Verezzi cave sediments and six filters from Po River water were observed by an expert operator with a UV flashlight (Alonefire SV10 365 nm UV flashlight 5W) under a Leitz ORTHOLUX II POL-MK microscope equipped with a DeltaPix Invenio 12EIII 12 Mpx Camera, with 2.5x, 4x, 10x zoom or more (Balestra and Bellopede, 2022). Particles that could not be identified as MPs were not taken into consideration. Moreover, microplastics were directly counted and measured on ImageJ, using the photos taken on 12 real sample filters and six images created with an image editing software, and compared to the data obtained using visual identification under a microscope. Visual counting of MPs on filters under a microscope and MP counting on photos using ImageJ were used to test and validate the developed image analysis method, setting the different parameters to reach a maximum 15% deviation for each filter.

2.3. Processing of the filter images

Different approaches may be employed for automatizing the detection of fluorescent microplastic on a filter. The simplest one consists of the manual color thresholding of the image, but this may lead to the omission of some microplastics from the count since the fluorescence intensity is variable for the different polymers and can be influenced by the presence of contaminations on the microplastic surface.

For the same reason, automatic thresholding techniques are also not applicable and can lead to very confounding results (see Supplementary Information Figure S1).

Automatic local thresholding algorithms, which apply a different threshold to different portions of the image determined based on local information of the pixels, could represent a viable solution. Unfortunately, the presence of strong halos around some fluorescent plastics leads to the failure of this class of techniques (see Supplementary Information Figure S2). Due to the limitations of the above-mentioned segmentation techniques, a more elaborate approach is required for the automatic segmentation of the microplastic filter images.

181 This work introduces and validates a novel segmentation technique based on the Canny edge detection
182 algorithm (Russ, 2016) that overcomes the problem of low-intensity fluorescent fibers and fluorescence
183 halos. Fluorescent pixels due to the presence of halo on MP photos under UV light are generally considered
184 by existing automatic counting programs, generating a size and shape error in the counted MPs. In fact,
185 instead of thresholding the image according to pixel intensity, the Canny algorithm works on its gradient.
186 After the gradient calculation, a non-maximum suppression step removes pixels that are likely to be
187 redundant and not part of an edge, and the image is finally thresholded according to a hysteresis threshold
188 method (Nixon, 2013). Moreover, morphological information such as length, thickness, and shape factor
189 are calculated for each microplastic which is eventually categorized as particle, fragment, or fiber.
190

191 **2.4. Development of a tool for the automated processing of sample images**

192 The processing of the images has been performed through a specifically made Python script named
193 *MicroplasticLab* (MUPL), mainly based on *OpenCV* ("Open CV Releases," n.d.) and *SkImage* ("Installing
194 scikit-image — skimage v0.19.2 docs," n.d.) libraries. MUPL is released as open-source software under
195 MIT license and provided with a web-based graphical user interface, shown in Figure 1, powered by the
196 open-source app framework Streamlit (Richards, 2021; "Streamlit • The fastest way to build and share data
197 apps," n.d.). The aim is to provide researchers and lab analysts with complete support, and for that, the
198 software also contains some functionalities to prepare the picture for publications, e.g., cropping, adding a
199 reference bar, etc. To ensure high performance and minimize processing time, MUPL has been designed
200 for running its functions, where possible, under Numba Compiler ("Numba: A High Performance Python
201 Compiler," n.d.).

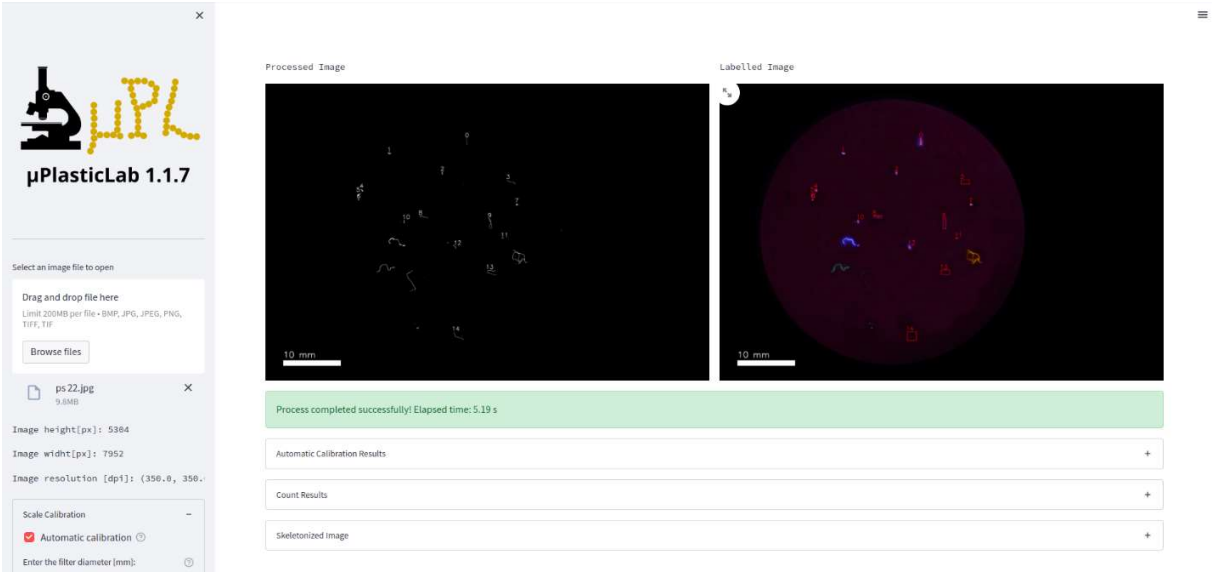

Figure 1: The user interface of MUPL running in a web browser. The results of processing the pictures acquired in the frame of this work are shown in the figure.

2.5. Automatic Detection of Scale Factor

The computation of the scale factor is undoubtedly required to convert the measurements performed on the image from pixel number to a unit of length, i.e., mm. MUPL offers the double possibility of manually entering a predetermined scale factor or automatically calculating it from the image if the filter membrane diameter (in millimeters) is entered.

The automatic determination process, summarized in Figure 2, is based on the grayscale conversion and subsequent image thresholding by computing the threshold value according to the entropy method proposed by Li (Li and Lee, 1993; Sezgin and Sankur, 2004) to remove all the features but the filter membrane background. At this point, the Hough transform allows determining both the center and the diameter of the membrane background. The calibration factor is therefore computed as the ratio between the diameter of the filter estimated by the Hough Transform (in pixels) and the actual diameter entered by the user (in millimeters).

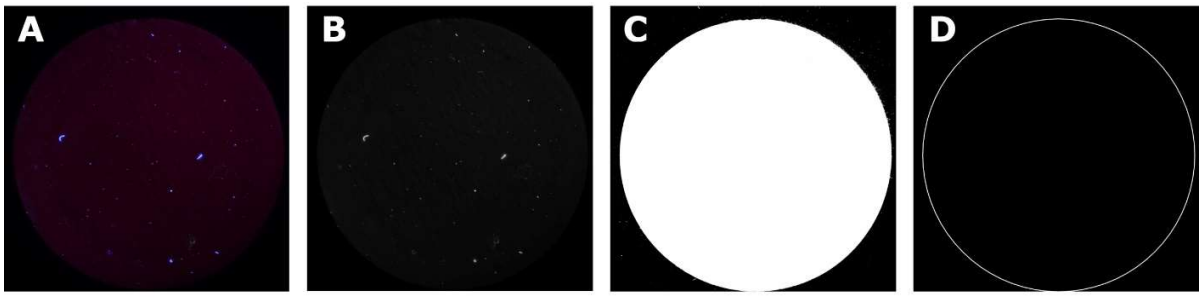

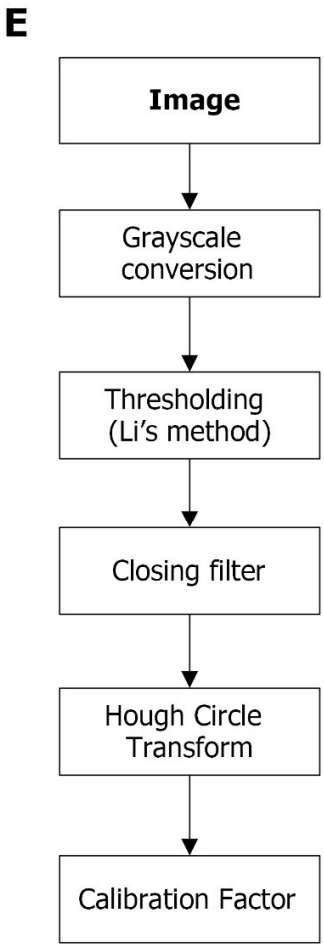

218

219 **Figure 2:** Example of automatic detection of the filter in an image. The original image A) is converted to
220 grayscale colorspace B) and thresholded with thresh value 5 C). In D) the contour of the membrane is
221 determined by the Hough Transform. E) Workflow for the automatic determination of the calibration factor.

222

2.6. Preliminary processing

The sample images often contain a certain amount of noise which is generally due to the presence of nanoplastics or fluorescent mineralogic fractions and can lead to a considerable overestimation in the microplastic count.

Mean and median morphological low pass filters have proven to be relatively ineffective in achieving noise-selective removal, and bandpass filtering in the frequency domain (Russ, 2016) has been chosen as a valid alternative. Examples of a gaussian bandpass filter on removing image noise originating from fluorescent mineralogic fraction on a microplastic filter image are shown in Figures S3 and Figure S4.

MUPL allows the user to enable Gaussian bandpass filter H in the following form:

$$H = exp\left\{-\frac{\left[d(f_x, f_y) - f_0\right]^2}{f_w^2}\right\}$$

Where $d^2(f_x, f_y)$ are the frequencies in the x and y direction, respectively, f_0 and f_w are respectively the center and the width of the bandpass filter.

Aiming at filtering all the features whose length is lower than l_{min} or great than l_{max} ,the corresponding Gaussian bandpass filter characteristics are calculated as follows:

$$f_0 = \frac{1}{2}\left(\frac{1}{l_{max}} + \frac{1}{l_{min}}\right)$$

$$f_w = \frac{1}{l_{max}} - \frac{1}{l_{min}}$$

After this optional removal step, the image background, mainly consisting of the glass filter, is removed by subtracting its blurred version obtained with a large radius median filter from the original image.

2.7. Detection and count of microplastics

We chose to detect and measure only fibers whose length ranges from 0.4 mm to 10 mm. The lower limit is imposed because the image resolution does not allow reliable identification of smaller

246 microplastics with the risk of including noise or other non-plastic particles in the counts. In general, to
247 avoid errors due to poor picture resolution, we highly recommend processing pictures which a scale factor
248 not lower than 100 pixels/mm; otherwise, the lower length detection limit should be increased.
249 Due to the presence of fibers of different materials, each of which produces a different fluorescent
250 response when exposed to an ultraviolet (UV) lamp, each color channel requires a separate treatment. A
251 thresholding approach on the grayscale version of the image has proven to be rather ineffective as the
252 fibers with low fluorescent emission are lost (See Supplementary Information Figure S4). Local and
253 adaptive thresholding techniques give inadequate results for a particle with high-intensity fluorescence
254 that can saturate the camera detector and produce the typical halo.
255 The workflow and results of the method we propose are presented in Figures 3 and 4. Such a method
256 is based on the segmentation of the separate color channels. Once the image is decomposed in its RGB
257 colorspace channels, the background for each of these is calculated through a wide radius median filter
258 and then subtracted from the initial image. To further limit the presence of fluorescence halos, a Canny
259 filter is also applied to the image to extract the boundaries of each fiber. The three channels are then
260 summed together, and the image is binarized by employing a thresholding operation. Finally, a closing
261 filter is applied to remove holes within the fiber area left by the Canny filter.
262 The skeletonization operations reduce each fiber to a 1-pixel wide binary representation whose area is
263 equal to the fiber length. Despite that, identifying each fiber as a separate entity also requires a connected
264 components analysis, easily obtained by the *connectedComponentsWithStats* ("OpenCV: Structural
265 Analysis and Shape Descriptors," n.d.) OpenCV function.
266 The thickness of the fiber is computed by dividing the area (number of non-zero pixels) in the
267 thresholded image before skeletonization within the fiber bounding box by its length. An example of size
268 and shape statistics generated by MUPL on the Po River sample set is reported in Figure S5.
269 All the values are converted to millimeters by dividing by the scale factor and rounded to 2 decimal
270 digits.
271

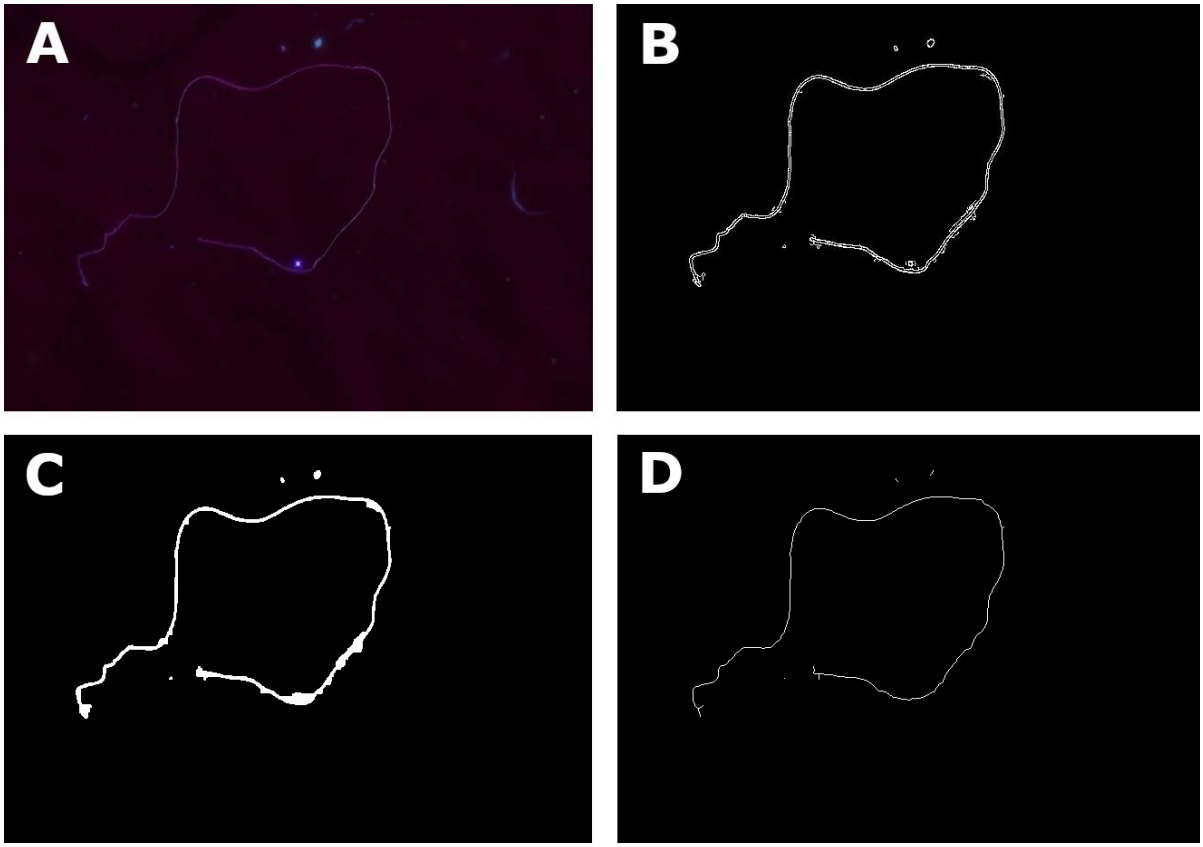

Figure 3: Sequence of image processing operations on a sample image. Original image of a microplastic fiber observed under UV light A). The same image after background removal and edge detection B), after a closing filter C) and after skeletonization D).

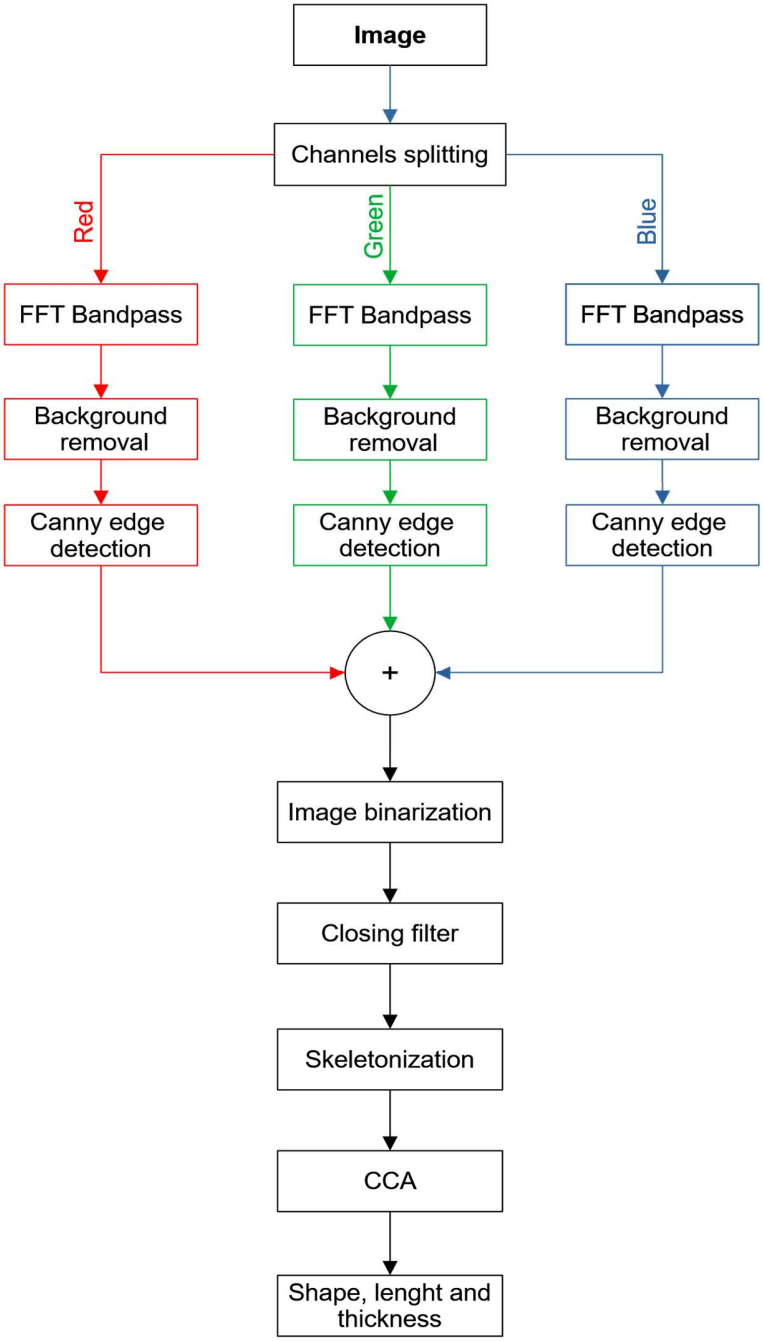

Figure 4: Workflow for the segmentation of UV-fluorescent microplastics on a filter.

3. Results and discussions

The first tests were carried out on the six images artificially created with an image editing software (Table 1). For each dataset, the deviation is defined as the percentage difference between the counts obtained by the operator visual count and the counts returned by MUPL. The automated count results on each sample set turn out to be quite accurate, returning a deviation smaller than 13.3% on each filter and an average absolute deviation below 8% (Table 1). The correlation between the visual count and the automated MUPL is reported in the graph of Fig. 5.

Table 1. Microplastic abundance under UV light on filters created with an image editing software MUPL set parameters: Background removal filter 30, Canny lower threshold 150, Canny upper threshold 210, Close filter size 3, Close filter size iterations 1.

Filter Sample	ImageJ Count	MUPL Count	Deviation [%]
PS-1	21	23	9.5
PS-2	15	13	-13.3
PS-3	18	20	11.1
PS-4	20	20	0.0
PS-5	14	15	7.1
PS-6	19	18	-5.3
Average	17.8	18.2	1.5

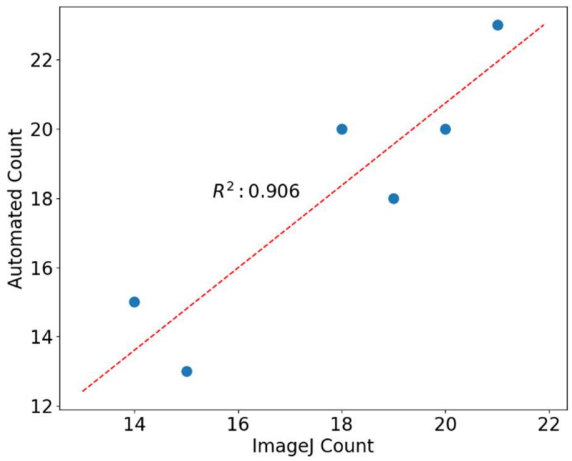

Figure 5. Correlation of MUPL Automated Count against ImageJ Count for the sample artificially produced with an image editing software.

Microplastics were found in all sediment samples of Borgio Verezzi show cave and in all water samples of Po River (Table 2,3). The automated count results on each sample set turn out to be quite accurate, returning a deviation of less than 15% on each filter and an average absolute deviation below 11% (Table 2,3). An exception is the single filter BV5, whose deviation is 29.4%. The correlation between the visual count and the automated MUPL for the samples from Borgio Verezzi show cave and Po River are reported in the graphs of Fig. 6 and 7 respectively. In the figures, it is also reported the correlation between the two types of counting for the Nile Red stained MPs.

Considering the mean value, the count error was further reduced when processing stained sample images: from 10.9% to 8% for Borgio Verezzi samples and from 8.3% to 6.9% for Po River samples (Table 2,3). Figures 5, 6 and 7 correlate the Automated count and ImageJ determination with regression coefficient calculation on the different samples without and with Nile Red staining. A summary of the count deviation obtained with MUPL for each sample is summarized in Figure 8.

Table 2. Microplastic abundance on filters of Borgio Verezzi show cave sediments [items/20 g of superficial sediment] under UV light. MUPL set parameters: Background removal filter 15, Canny lower threshold 100, Canny upper threshold 155, Close filter size 5, Close filter size iterations 1. UV photo with Nile Red: Background removal filter 10, Canny lower threshold 230, Canny upper threshold 230, Close filter size 3, Close filter size iterations 1.

Filter Sample	**ImageJ Count**	**MUPL Count**	**Deviation [%]**	**MUPL Count (Stained)**	**Deviation (Stained) [%]**
BV-1	10	10	0.0	11	10.0
BV-2	25	22	-12.0	22	-12.0
BV-3	21	24	14.3	20	-4.8
BV-4	13	13	0.0	15	15.4
BV-5	17	12	-29.4	16	-5.9
BV-6	10	11	10.0	10	0.0
Average	16.0	15.3	10.9	15.7	8.0

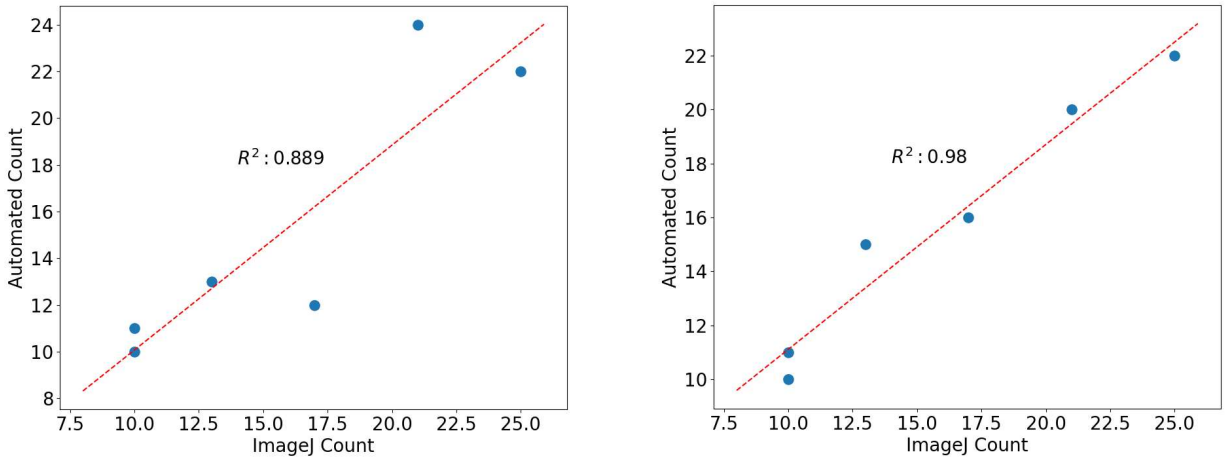

Figure 6. Correlation of MUPL Automated Count vs ImageJ Count for the sample of sediment of Borgio Verezzi show cave without (A) and with (B) Nile Red staining.

Table 3. Microplastic abundance on filters of Po River water [items/L of shallow water] under UV light. MUPL set parameters: Background removal filter 30, Canny lower threshold 150, Canny upper threshold 210, Close filter size 3, Close filter size iterations 1. MUPL set parameters with Nile Red: Background removal filter 15, Canny lower threshold 195, Canny upper threshold 230, Close filter size 3, Close filter size iterations 1.

Filter	ImageJ Count	MUPL Count	Deviation [%]	MUPL Count (Stained)	Deviation (Stained) [%]
PO-1	84	77	8.3	90	7.1
PO-2	31	28	9.7	34	9.7
PO-3	24	24	0.0	21	12.5
PO-4	18	20	11.1	18	0.0
PO-5	44	40	9.1	39	11.4
PO-6	34	38	11.8	34	0.0
Average	39.2	37.8	8.3	39.3	6.8

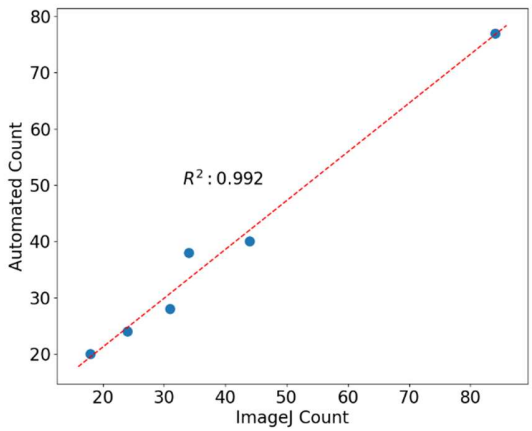

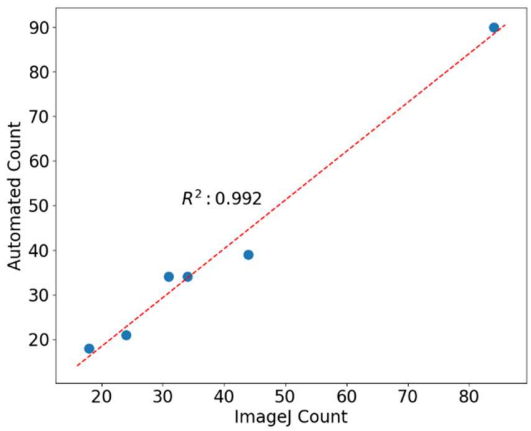

329 **Figure 7.** Correlation of MUPL Automated Count vs ImageJ Count for the sample of Po River water
330 without (A) and with (B) Nile Red staining.
331 The use of Nile Red dye has not made substantial improvements in the MPs coloring; however, it has
332 improved and uniformed the filter background allowing a better distinction of the plastic material on the
333 filters. Moreover, the results indicate that staining with Nile Red dye reduced the average deviation on both
334 Borgio Verezzi and Po River samples. This can be related to the fact that the majority of MPs found on our
335 filters were synthetic fibers, often made of polyester materials, which are hard to stain. However, under UV
336 exposure, these fibers presented a strong fluorescence under UV light due to the presence of FWAs, making
337 them easy to identify.

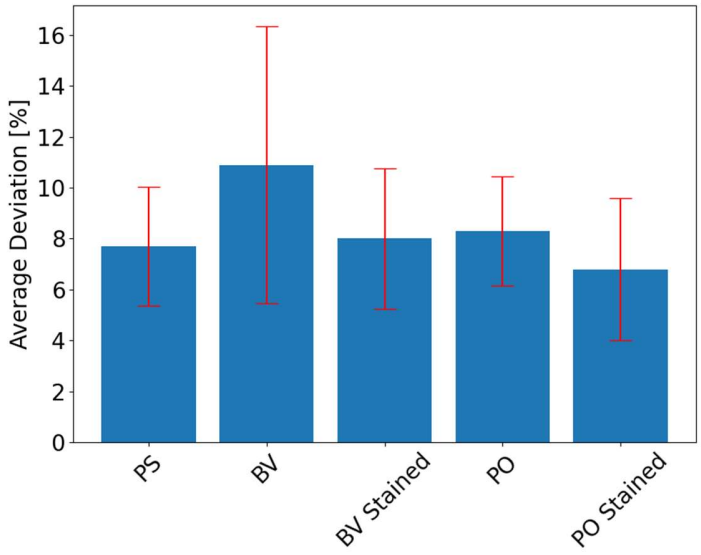

338

339 **Figure 8.** Summary of MUPL count deviations for each sample. The blue bars represent the average of
340 absolute deviation; the red bar represents the range of deviation that comprises all the processed filter
341 images.

342

343 The MP abundance value found in the first six Borgio Verezzi show cave samples examined (about 500-
344 1250 items/kg) is very small compared to those found in Bossea show cave sediments (2500-8700 items/kg

345 along the tourist path and 1600 items/kg in the speleological area) (Balestra and Bellopede, 2022).
346 However, the Bossea show cave values have been calculated considering fluorescent and not-fluorescent
347 MPs, and a 12.3% of the total MPs in this cave sediments were not fluorescent. Therefore, it is reasonable
348 to consider for Borgio Verezzi cave at least 10% more MPs than the value obtained with the counting of
349 fluorescent particles.
350 The MP abundance value found in the Po River water samples (about 18-84 items/L) are similar to those
351 found in the Gallatin River, USA (0.001-67.5 items/L) (Barrows et al., 2018), and relatively high compared
352 to those found in the Yangtze River Estuary water, China (0,5-10,2 items/L) (Zhao et al., 2014) or
353 Amsterdam canal water, Netherland (4.8-18.7 items/L) (Leslie et al., 2017). The large amount of MPs found
354 in the Po River could be linked to the different methods used or to the sampling place on shore, where the
355 currents are less noticeable and, therefore, an accumulation may occur.
356

357 **4. CONCLUSIONS**

358 The importance of image analysis for the recognition of microplastics is linked to the rapidity of the process
359 and could lead to the detection of microplastics directly in situ. Existing detection methodologies often
360 require a long processing time and specific dedicated equipment. The complexity of the real samples
361 highlighted the necessity to remove organic matter and take photos of high quality for better image analysis.
362 The new software proposed in this work, MicroplasticLab (MUPL), uses an approach for the automatic
363 segmentation of the image and solves the halo problem that can be found around the fluorescent particles.
364 This fact avoids identification errors and misattribution of microplastic shapes. This software can be used
365 on filters photographed under UV light with and without using a staining dye. The results obtained with
366 this software on images of real samples gave an average deviation on a single filter of less than 15.4%.
367 If we consider the whole set of filters within the same sample set, the deviation is, on the stained samples,
368 always lower than 10%.
369 For these reasons, MicroplasticLab can undoubtedly provide useful and reliable support for quantifying
370 microplastic pollution in different environments and matrices, paving the way for a new semiautomated

approach. Moreover, its capability of producing statistical information on the size and shape of the detected particles can help detecting their sources and assist in establishing removal strategies.

The proposed process can also filter the presence of fluorescent mineralogic particles by a Fast Fourier Transform (FFT) filter which might affect the overall count in some cases. To improve microplastic recognition for these cases, further investigation should explore the possibility of using digestion techniques that combine biological and inorganic fraction removal.

MicroplasticLab is conceived as a tool to help the environmental researcher to identify and estimate the contamination from microplastics in different environments. At the same time, identification of the type of plastic is of great importance for a complete analysis. In this direction, an improvement would be to couple the MUPL technique with some algorithm for identifying the microplastics based on a particle-by-particle spectroscopic analysis directed to microplastics automatically identified by the software. In this way, with a quick analysis of a filter membrane, the researcher could count, measure, and identify the nature of MP particles.

ASSOCIATED CONTENT

-SupportingInfo.pdf (PDF): contains additional images of microplastic samples processed in Fiji showing results of Automatic thresholding techniques. It also includes an example of an FFT bandpass filter on a sample image and examples of size/shape statistics generated by MUPL.

-MUPL_sourcecode.zip: contains the source code of MUPL Python script. The main user interface can be run, upon installation of required dependencies, by typing in the system terminal the following command *streamlit run Main.py*

-MUPLTutorial.pdf: quick tutorial to show how to process microplastic on membrane filter imges on MUPL.

ACKNOWLEDGMENTS

The authors are grateful to the Borgio Verezzi cave managers, that allowed us to collect samples for our research, and Paolo Felice Maschio and Nives Grasso (DIATI, Politecnico di Torino) for lending us the photographic equipment.

This work was realized within the research project ""SHOWCAVE: a multidisciplinary research project to study, classify and mitigate the environmental impact in tourist caves"", funded by the Italian Ministry of Education, University and Research [PRIN: Progetti di ricerca di rilevante interesse nazionale 2017 - Prot. 2017HTXT2R; PI: Prof. Marco Isaia, University of Torino].

The authors also acknowledge support from CleanWaterCenter (CWC) @ PoliTO.

ABBREVIATIONS

MP microplastic, MPs microplastics, MUPL MicroplasticLab, UV ultraviolet

REFERENCES

Alomar, C., Estarellas, F., Deudero, S., 2016. Microplastics in the Mediterranean Sea: Deposition in coastal shallow sediments, spatial variation and preferential grain size. Marine Environmental Research 115, 1–10. https://doi.org/10.1016/j.marenvres.2016.01.005

Balestra, V., Bellopede, R., 2022. Microplastic pollution in show cave sediments: First evidence and detection technique. Environmental Pollution 292, 118261. https://doi.org/10.1016/j.envpol.2021.118261

Barboza, L.G.A., Dick Vethaak, A., Lavorante, B.R.B.O., Lundebye, A.-K., Guilhermino, L., 2018. Marine microplastic debris: An emerging issue for food security, food safety and human health. Marine Pollution Bulletin 133, 336–348. https://doi.org/10.1016/j.marpolbul.2018.05.047

Boyle, K., Örmeci, B., 2020. Microplastics and Nanoplastics in the Freshwater and Terrestrial Environment: A Review. Water 12, 2633. https://doi.org/10.3390/w12092633

420 Cannas, S., Fastelli, P., Guerranti, C., Renzi, M., 2017. Plastic litter in sediments from the coasts of south
421 Tuscany (Tyrrhenian Sea). Marine Pollution Bulletin 119, 372–375.
422 https://doi.org/10.1016/j.marpolbul.2017.04.008
423 Chia, R.W., Lee, J.-Y., Kim, H., Jang, J., 2021. Microplastic pollution in soil and groundwater: a review.
424 Environ Chem Lett 19, 4211–4224. https://doi.org/10.1007/s10311-021-01297-6
425 Corami, F., Rosso, B., Bravo, B., Gambaro, A., Barbante, C., 2020. A novel method for purification,
426 quantitative analysis and characterization of microplastic fibers using Micro-FTIR. Chemosphere
427 238, 124564. https://doi.org/10.1016/j.chemosphere.2019.124564
428 Crawford, C.B., Quinn, B., 2016. Microplastic Pollutants. Elsevier.
429 Cutroneo, L., Reboa, A., Besio, G., Borgogno, F., Canesi, L., Canuto, S., Dara, M., Enrile, F., Forioso, I.,
430 Greco, G., Lenoble, V., Malatesta, A., Mounier, S., Petrillo, M., Rovetta, R., Stocchino, A.,
431 Tesan, J., Vagge, G., Capello, M., 2020. Microplastics in seawater: sampling strategies,
432 laboratory methodologies, and identification techniques applied to port environment. Environ Sci
433 Pollut Res 27, 8938–8952. https://doi.org/10.1007/s11356-020-07783-8
434 Ehlers, S.M., Maxein, J., Koop, J.H.E., 2020. Low-cost microplastic visualization in feeding experiments
435 using an ultraviolet light-emitting flashlight. Ecological Research 35, 265–273.
436 https://doi.org/10.1111/1440-1703.12080
437 Erni-Cassola, G., Gibson, M.I., Thompson, R.C., Christie-Oleza, J.A., 2017. Lost, but Found with Nile
438 Red: A Novel Method for Detecting and Quantifying Small Microplastics (1 mm to 20 μm) in
439 Environmental Samples. Environ. Sci. Technol. 51, 13641–13648.
440 https://doi.org/10.1021/acs.est.7b04512
441 Esch, E. von der, Kohles, A.J., Anger, P.M., Hoppe, R., Niessner, R., Elsner, M., Ivleva, N.P., 2020.
442 TUM-ParticleTyper: A detection and quantification tool for automated analysis of (Microplastic)
443 particles and fibers. PLOS ONE 15, e0234766. https://doi.org/10.1371/journal.pone.0234766

444 Gauci, A., Deidun, A., Montebello, J., Abela, J., Galgani, F., 2019. Automating the characterisation of
445 beach microplastics through the application of image analyses. Ocean & Coastal Management
446 182, 104950. https://doi.org/10.1016/j.ocecoaman.2019.104950
447 Guerranti, C., Cannas, S., Scopetani, C., Fastelli, P., Cincinelli, A., Renzi, M., 2017. Plastic litter in
448 aquatic environments of Maremma Regional Park (Tyrrhenian Sea, Italy): Contribution by the
449 Ombrone river and levels in marine sediments. Marine Pollution Bulletin 117, 366–370.
450 https://doi.org/10.1016/j.marpolbul.2017.02.021
451 Ha, J., Yeo, M.-K., 2018. The environmental effects of microplastics on aquatic ecosystems. Mol. Cell.
452 Toxicol. 14, 353–359. https://doi.org/10.1007/s13273-018-0039-8
453 Henry, B., Laitala, K., Klepp, I.G., 2018. Microplastic pollution from textiles: A literature review.
454 Hidalgo-Ruz, V., Gutow, L., Thompson, R.C., Thiel, M., 2012. Microplastics in the Marine Environment:
455 A Review of the Methods Used for Identification and Quantification. Environ. Sci. Technol. 46,
456 3060–3075. https://doi.org/10.1021/es2031505
457 Huang, J., Chen, H., Zheng, Y., Yang, Y., Zhang, Y., Gao, B., 2021. Microplastic pollution in soils and
458 groundwater: Characteristics, analytical methods and impacts. Chemical Engineering Journal 425,
459 131870. https://doi.org/10.1016/j.cej.2021.131870
460 Installing scikit-image — skimage v0.19.2 docs [WWW Document], n.d. URL https://scikit-
461 image.org/docs/stable/install.html (accessed 7.3.22).
462 Klein, M., Fischer, E.K., 2019. Microplastic abundance in atmospheric deposition within the
463 Metropolitan area of Hamburg, Germany. Science of The Total Environment 685, 96–103.
464 https://doi.org/10.1016/j.scitotenv.2019.05.405
465 Li, C.H., Lee, C.K., 1993. Minimum cross entropy thresholding. Pattern Recognition 26, 617–625.
466 https://doi.org/10.1016/0031-3203(93)90115-D
467 Liu, Y., Sun, P., Wergeles, N., Shang, Y., 2021. A survey and performance evaluation of deep learning
468 methods for small object detection. Expert Systems with Applications 172, 114602.
469 https://doi.org/10.1016/j.eswa.2021.114602

Lorenzo-Navarro, J., Castrillón-Santana, M., Sánchez-Nielsen, E., Zarco, B., Herrera, A., Martínez, I., Gómez, M., 2021. Deep learning approach for automatic microplastics counting and classification. Science of The Total Environment 765, 142728. https://doi.org/10.1016/j.scitotenv.2020.142728

Lorenzo-Navarro, J., Castrillón-Santana, M., Santesarti, E., De Marsico, M., Martínez, I., Raymond, E., Gómez, M., Herrera, A., 2020. SMACC: A System for Microplastics Automatic Counting and Classification. IEEE Access 8, 25249–25261. https://doi.org/10.1109/ACCESS.2020.2970498

Mathalon, A., Hill, P., 2014. Microplastic fibers in the intertidal ecosystem surrounding Halifax Harbor, Nova Scotia. Marine Pollution Bulletin 81, 69–79. https://doi.org/10.1016/j.marpolbul.2014.02.018

Mukhanov, V.S., Litvinyuk, D.A., Sakhon, E.G., Bagaev, A.V., Veerasingam, S., Venkatachalapathy, R., 2019. A new method for analyzing microplastic particle size distribution in marine environmental samples. Ecologica Montenegrina 23, 77–86. https://doi.org/10.37828/em.2019.23.10

Nixon, M., 2013. Feature Extraction and Image Processing. Elsevier.

Numba: A High Performance Python Compiler [WWW Document], n.d. URL https://numba.pydata.org/ (accessed 7.3.22).

Open CV Releases, n.d. . OpenCV. URL https://opencv.org/releases/ (accessed 7.3.22).

OpenCV: Structural Analysis and Shape Descriptors [WWW Document], n.d. URL https://docs.opencv.org/3.4/d3/dc0/group__imgproc__shape.html (accessed 7.15.22).

Prata, J.C., Alves, J.R., da Costa, J.P., Duarte, A.C., Rocha-Santos, T., 2020. Major factors influencing the quantification of Nile Red stained microplastics and improved automatic quantification (MP-VAT 2.0). Science of The Total Environment 719, 137498. https://doi.org/10.1016/j.scitotenv.2020.137498

Prata, J.C., Reis, V., Matos, J.T.V., da Costa, J.P., Duarte, A.C., Rocha-Santos, T., 2019. A new approach for routine quantification of microplastics using Nile Red and automated software (MP-VAT).

Science of The Total Environment 690, 1277–1283. https://doi.org/10.1016/j.scitotenv.2019.07.060

Qiu, Q., Peng, J., Yu, X., Chen, F., Wang, J., Dong, F., 2015. Occurrence of microplastics in the coastal marine environment: First observation on sediment of China. Marine Pollution Bulletin 98, 274–280. https://doi.org/10.1016/j.marpolbul.2015.07.028

Ren, Z., Gui, X., Xu, X., Zhao, L., Qiu, H., Cao, X., 2021. Microplastics in the soil-groundwater environment: Aging, migration, and co-transport of contaminants – A critical review. Journal of Hazardous Materials 419, 126455. https://doi.org/10.1016/j.jhazmat.2021.126455

Richards, T., 2021. Getting Started with Streamlit for Data Science: Create and deploy Streamlit web applications from scratch in Python. Packt Publishing Ltd.

Russ, J.C., 2016. The Image Processing Handbook. CRC Press.

Samandra, S., Johnston, J.M., Jaeger, J.E., Symons, B., Xie, S., Currell, M., Ellis, A.V., Clarke, B.O., 2022. Microplastic contamination of an unconfined groundwater aquifer in Victoria, Australia. Science of The Total Environment 802, 149727. https://doi.org/10.1016/j.scitotenv.2021.149727

Sezgin, M., Sankur, B., 2004. Survey over image thresholding techniques and quantitative performance evaluation. JEI 13, 146–165. https://doi.org/10.1117/1.1631315

Sharma, S., Chatterjee, S., 2017. Microplastic pollution, a threat to marine ecosystem and human health: a short review. Environ Sci Pollut Res 24, 21530–21547. https://doi.org/10.1007/s11356-017-9910-8

Streamlit • The fastest way to build and share data apps [WWW Document], n.d. URL https://streamlit.io/ (accessed 7.18.21).

Theuwissen, A.J.P., 2008. Influence of Terrestrial Cosmic Rays on the Reliability of CCD Image Sensors—Part 2: Experiments at Elevated Temperature. IEEE Transactions on Electron Devices 55, 2324–2328. https://doi.org/10.1109/TED.2008.927662

519 Theuwissen, A.J.P., 2007. Influence of Terrestrial Cosmic Rays on the Reliability of CCD Image
520 Sensors—Part 1: Experiments at Room Temperature. IEEE Transactions on Electron Devices 54,
521 3260–3266. https://doi.org/10.1109/TED.2007.908906
522 Wegmayr, V., Sahin, A., Sæmundsson, B., Buhmann, J., 2020. Instance Segmentation for the
523 Quantification of Microplastic Fiber Images. 2020 IEEE Winter Conference on Applications of
524 Computer Vision (WACV). https://doi.org/10.1109/WACV45572.2020.9093352
525 Zhang, C., Zhou, H., Cui, Y., Wang, C., Li, Y., Zhang, D., 2019. Microplastics in offshore sediment in
526 the Yellow Sea and East China Sea, China. Environmental Pollution 244, 827–833.
527 https://doi.org/10.1016/j.envpol.2018.10.102
528